A Simple Chaotic System With Topologically Different Attractors

KARTHIKEYAN RAJAGOPAL[1], AKIF AKGUL[ID][2], IRENE M. MOROZ[3], ZHOUCHAO WEI[4], SAJAD JAFARI[5], AND IQTADAR HUSSAIN[ID][6]

[1]Centre for Non-Linear Dynamics, Defence University, Bishoftu, Ethiopia
[2]Department of Electrical and Electronics Engineering, Sakarya University of Applied Sciences, 54050 Sakarya, Turkey
[3]Mathematical Institute, University of Oxford, Oxford OX2 6GG, U.K.
[4]School of Mathematics and Physics, China University of Geosciences, Wuhan 430074, China
[5]Nonlinear Systems and Applications, Faculty of Electrical and Electronics Engineering, Ton Duc Thang University, Ho Chi Minh 758307, Vietnam
[6]Department of Mathematics, Statistics and Physics, Qatar University, Doha 2713, Qatar

Corresponding author: Iqtadar Hussain (iqtadarqau@qu.edu.qa)

ABSTRACT There have been many different investigations of nonlinear dynamical systems. In this paper, we introduce a new chaotic system. In the proposed system, the attractor can be modified by adding a nonlinear term to the third state equation, thereby generating six different self-excited chaotic attractors. Some dynamical properties such as Hopf bifurcation, bifurcation diagrams, and multistability of the proposed system are investigated. The new system shows topologically different attractors for all six cases. We investigate two cases in depth. We also use nonlinear feedback control to drive the system to equilibrium, using two cases for illustration.

INDEX TERMS Chaotic systems, self-excited attractor, hidden attractor, multistability, nonlinear feedback control.

I. INTRODUCTION

After the discovery of the well-known Lorenz system [1], the past few decades have seen many papers discussing deterministic chaotic models [2], [3]. Chaotic attractors are characterized by features such as strong dependence on initial conditions, sensitivity to the changes in the system's parameters, the presence of strong harmonics in the signals, the fractional dimension of space state trajectories, and the presence of stretching directions represented by a positive Lyapunov exponent.

It has been of great interest to design chaotic attractors with unique features. For example, systems with multi-wing attractors [4]–[6], memristive chaotic systems [7]–[9], hyperchaotic systems [10], systems with fractional order [11], [12], systems which are megastable [13]–[15], and systems with extreme multi-stability [16]–[18].

Recently researchers have proposed chaotic attractors with self-excited and hidden attractors [19]–[22]. A self-excited attractor has a basin of attraction containing an unstable equilibrium, while this is not the case in hidden

The associate editor coordinating the review of this manuscript and approving it for publication was Sun Junwei.

attractors [23]–[25]. Several papers [23], [26], [27] by Kuznetsov and Leonov provided a platform to understand hidden attractors and their influence on real-time systems. Chaotic attractors with hidden oscillations can be seen in systems with no equilibrium [28], with only stable equilibria [29] and with curves of equilibria [30], [31].

Chaotic reversal systems have been discussed in the literature in the past decade. Many natural and experimental models show such reversal behaviors like the Lorenz system [1], Rossler system [32], the Sprott models [33], and so on. Gissinger *et al.* [34] proposed a new model of chaotic reversal for a turbulent magnetic dynamo, whose dynamics are of a stochastic nature. Recently many papers have discussed chaotic attractors of memristor circuits dealing with infinite equilibria [35] and hybrid chaotic circuits with memristors [36]. A two-memristor-based hyperchaotic system with a plane of equilibria and the initial boosting phenomenon was discussed in [37]. A chaotic memristor oscillator with hypogenetic jerk equations was proposed in [31], and this system has a line of equilibria and long term transient period. A state variable method was used to study the memristor system with a line of equilibrium in [38] and a memristor system with extreme multistability was discussed

TABLE 1. The different cases of the system (2).

System name	Parameters				Fig.1
	d	c	b	a	
Case-1	0	0	0.1	0.2	a
Case-2	0	1	0.1	0.12	b
Case-3	0	0.5	0.115	0.12	e
Case-4	0.1	0	0.1	0.12	c
Case-5	0.1	0.001	0.1	0.1	d
Case-6	0.1	0.001	0.1	0.7	f

in [39]. It was Gissinger's paper [40], about chaotic reversal systems which motivated us to propose a new chaotic system derived from his model which can show topologically different strange attractors. The original system [36] is a chaotic reversal system with five equilibrium points and hence attracted our interest to analyze further the possibility of generating topologically different attractors. Our system has shown multistability and coexisting attractors compared to the original system [36].

In Section 2, the new chaotic system (NCS) is introduced, and its dynamical properties are analyzed in Section 3. In Sections 4, 5 and 6, Hopf bifurcation, bifurcation transitions diagrams and multistability of the proposed novel system are derived and investigated. In Section 7, nonlinear feedback control is applied to drive the system to equilibrium. The last section provides conclusions and future works.

II. NOVEL CHAOTIC SYSTEM (NCS)

A set of equations, proposed to show reversals of the Earth's geomagnetic field was discussed by [40]. The mathematical model takes the form:

$$\begin{cases} \dot{x} = ax - yz, \\ \dot{y} = -by + xz, \\ \dot{z} = c - z + xy. \end{cases} \quad (1)$$

System (1) gives a self-excited attractor with five equilibrium points, which is topologically different to other well-known systems such as the Lorenz and Rossler systems, which have three and two equilibria respectively. In this paper system (1) is modified by including an additional nonlinear term in the third state equation for z, thereby generating six different self-excited chaotic attractors, as given in Table 1. The mathematical model of the proposed new system is

$$\begin{cases} \dot{x} = ax - yz, \\ \dot{y} = -by + xz, \\ \dot{z} = c - z + xy + dzy, \end{cases} \quad (2)$$

where a,b,c,d are the parameters of the system. We term (2) the 'NCS'.

The cases shown in Table 1 are derived from system (2) for different parameter values,

For the initial conditions [0.1,0.1,0] and parameter values as shown in Table. 1, the phase portraits are shown
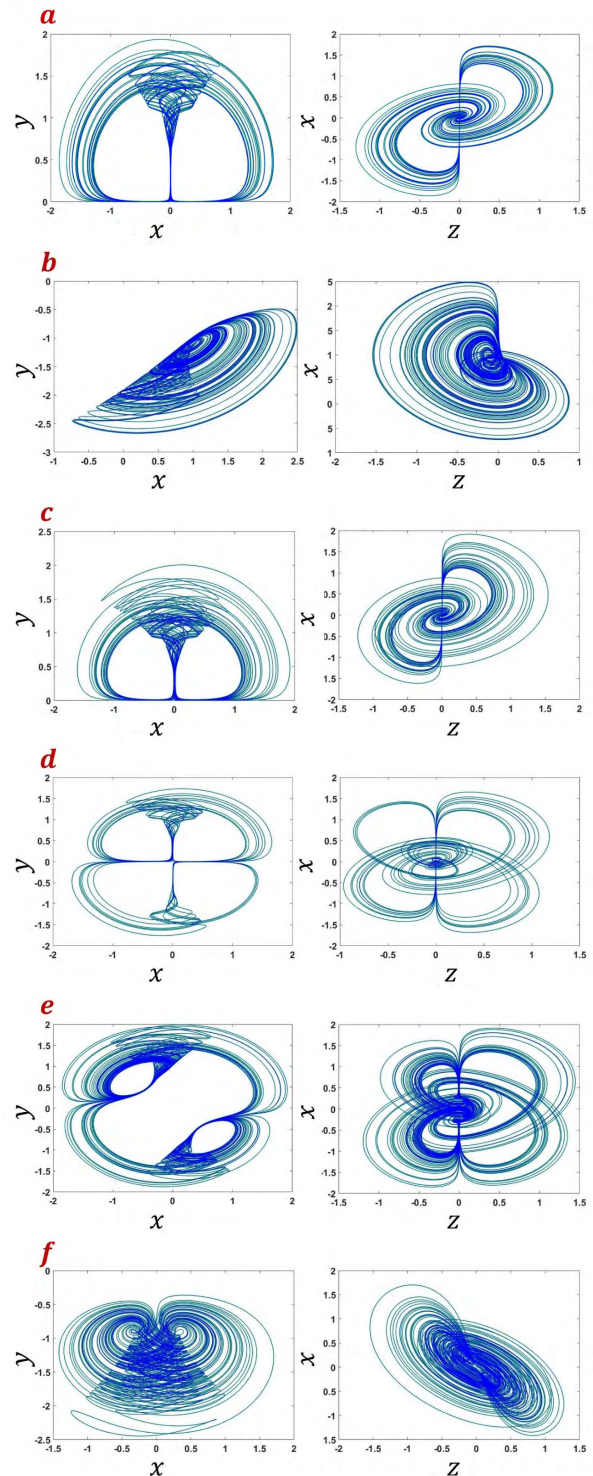
FIGURE 1. 2D phase portraits of the NCS for the different cases shown in Table 1.

in Fig.1 (a-f). It can be seen from the figures that the proposed NCS has topologically different attractors for all the six cases.

III. DYNAMIC PROPERTIES OF THE NCS

The five equilibrium points for the NCS for the parameter choices shown in Table 1 are given in Table 2 and 3. Various

TABLE 2. Equilibrium points of the NCS.

	x	y	z
E_1	0	0	c
E_2	$-\dfrac{\left[\sqrt{ab}\left(\frac{ad}{2}+\frac{\sqrt{\frac{4ab-4c\sqrt{ab}+a^2bd^2}{b}}}{2}\right)\right]}{a}$	$-\dfrac{ad}{2}-\dfrac{\sqrt{\frac{4ab-4c\sqrt{ab}+a^2bd^2}{b}}}{2}$	$\sqrt{ab}$
E_3	$-\dfrac{\left[\sqrt{ab}\left(\frac{ad}{2}-\frac{\sqrt{\frac{4ab-4c\sqrt{ab}+a^2bd^2}{b}}}{2}\right)\right]}{a}$	$-\dfrac{ad}{2}+\dfrac{\sqrt{\frac{4ab-4c\sqrt{ab}+a^2bd^2}{b}}}{2}$	$\sqrt{ab}$
E_4	$\dfrac{\left[\sqrt{ab}\left(\frac{ad}{2}+\frac{\sqrt{\frac{4ab-4c\sqrt{ab}+a^2bd^2}{b}}}{2}\right)\right]}{a}$	$-\dfrac{ad}{2}-\dfrac{\sqrt{\frac{4ab+4c\sqrt{ab}+a^2bd^2}{b}}}{2}$	$\sqrt{ab}$
E_5	$\dfrac{\left[\sqrt{ab}\left(\frac{ad}{2}-\frac{\sqrt{\frac{4ab-4c\sqrt{ab}+a^2bd^2}{b}}}{2}\right)\right]}{a}$	$-\dfrac{ad}{2}+\dfrac{\sqrt{\frac{4ab+4c\sqrt{ab}+a^2bd^2}{b}}}{2}$	$\sqrt{ab}$

TABLE 3. Eigenvalues of the NCS for different cases of table.1.

System Name	Equilibrium Points	Type of Equilibrium		
		λ_1	$\lambda_{2,3}$	
Case-1	(0, 0, 0)	-1	0, 0.2	Index-1 saddle node
	(0.3162,-0.4472,-0.1414)	-0.9828	$0.0414 \pm 0.2822i$	Saddle foci
	(-0.3162,0.4472,-0.1414)	-0.9828	$0.0414 \pm 0.2822i$	Saddle foci
	(-0.3162,-0.4472,0.1414)	-0.9828	$0.0414 \pm 0.2822i$	Saddle foci
	(0.3162,0.4472,0.1414)	-0.9828	$0.0414 \pm 0.2822i$	Saddle foci
Case-2	No equilibrium			
Case-3	No equilibrium			
Case-4	(0.3218, -0.3525, -0.1095)	-1.0557	$0.0202 \pm 0.2141i$	Saddle foci
	(-0.3108, 0.3405, -0.1095)	-0.9968	$0.0254 \pm 0.2160i$	Saddle foci
	(-0.3218, -0.3525, 0.1095)	-1.0557	$0.0202 \pm 0.2141i$	Saddle foci
	(0.3108, 0.3405, 0.1095)	-0.9968	$0.0254 \pm 0.2160i$	Saddle foci
	(0,0,0)	-1	-0.1, 0.12	Index-1 saddle node
Case-5	(0, 0, 0.001)	-1	-0.1, 0.1	0.12
	(0.3228, -0.3228, -0.1)	-1.0654	$0.0166 \pm 0.1956i$	Saddle foci
	(-0.3128, 0.3128, -0.1)	-1.0107	$0.0210 \pm 0.1972i$	Saddle foci
	(-0.3197,-0.3197, 0.1)	-1.0645	$0.0163 \pm 0.1938i$	Saddle foci
	(0.3097,0.3097, 0.1)	-1.0103	$0.0206 \pm 0.1954i$	Saddle foci
Case-6	(0.3303, -0.8740, -0.2646)	-0.8658	$0.1892 \pm 0.5504i$	Saddle foci
	(-0.3039, 0.8040, -0.2646)	-0.7756	$0.2280 \pm 0.5440i$	Saddle foci
	(-0.3291, -0.8708, 0.2646)	-0.8670	$0.1899 \pm 0.5475i$	Saddle foci
	(0.3027, 0.8008, 0.2646)	-0.7769	$0.2285 \pm 0.5408i$	Saddle foci
	(0,0, 0.001)	-1	-0.1, 0.7	Index-1 saddle node

self-excited chaotic attractors can be generated with different fixed points as shown in Table 3. We note that the system shows hidden oscillations for case-2 and case-3 where there are no real fixed points.

The finite time Lyapunov exponents (LEs) of the NCS are calculated using the Wolf's algorithm [41] for a finite time of 20000s. The initial conditions to calculate the LEs are [0.1,0.1,0] . Table 4 shows the LEs and the Kaplan-Yorke dimension all the six cases discussed in Table 1.

IV. HOPF BIFURCATION
To derive and investigate the Hopf bifurcation for the NCS, we choose case-1, where the parameter values are $a = 0.2$;

$b = 0.1$ and $c = 0$ and parameter d is considered as the control parameter. System (2) can have at most five equilibria:

$$A_1 = (0, 0, 0),$$
$$A_2 = (\frac{1}{20}(\sqrt{2}\sqrt{d^2+20}+\sqrt{2}d),$$
$$\frac{1}{10}(-\sqrt{d^2+20}-d), -\frac{1}{5\sqrt{2}}),$$
$$A_3 = (-\frac{1}{20}(\sqrt{2}\sqrt{d^2+20}+\sqrt{2}d),$$
$$\frac{1}{10}(-\sqrt{d^2+20}-d), \frac{1}{5\sqrt{2}}),$$

System Name	Lyapunov Exponents	Nature of system	Kaplan-Yorke Dimension D_{KY}
Case 1	0.024, 0, 0.924	Dissipative	2.025
Case 2	0.0898, 0, -1.06	Dissipative	2.084
Case 3	0.0558, 0, -1.05	Dissipative	2.053
Case 4	0.0153, 0, -0.97	Dissipative	2.015
Case 5	0.0104, 0, -1.002	Dissipative	2.010
Case 6	0.1211, 0, -0.625	Dissipative	2.194

$$A_4 = (\frac{1}{20}(\sqrt{2}d - \sqrt{2}\sqrt{d^2 + 20}),$$
$$\frac{1}{10}(\sqrt{d^2 + 20} - d), -\frac{1}{5\sqrt{2}}),$$
$$A_5 = (-\frac{1}{20}(\sqrt{2}d - \sqrt{2}\sqrt{d^2 + 20}),$$
$$\frac{1}{10}(\sqrt{d^2 + 20} - d), \frac{1}{5\sqrt{2}}), \quad (3)$$

It is not hard to check that there is no Hopf bifurcation at the origin and hence we consider a Hopf bifurcation analysis at the equilibrium point A_2. (We can derive analogous results for the other points.) The characteristic equation for linearised stability about A_2 is:

$$\frac{2}{25} + \frac{d^2}{250} + \frac{1}{250}d\sqrt{20 + d^2} + \left(\frac{d^2}{100} + \frac{1}{100}d\sqrt{20 + d^2}\right)\lambda$$
$$+ \left(\frac{9}{10} + \frac{d^2}{10} + \frac{1}{10}d\sqrt{20 + d^2}\right)\lambda^2 + \lambda^3 = 0 \quad (4)$$

Suppose that the characteristic equation of the system has a pair of imaginary roots $\pm i\omega$ ($\omega \in \Re^+$). It is not hard to show that when $d = d_0 = 1.1713341066595535$, (4) yields

$$\lambda_1 = -1.5781 < 0, \quad \lambda_{2,3} = \pm 0.26052i. \quad (5)$$

Taking d as the Hopf bifurcation parameter, the transversality condition

$$\Re(\lambda'(b_0))|_{\lambda=0.26052i} = -0.135742 < 0 \quad (6)$$

is satisfied. Therefore we get the following theorem.

Theorem 1:: If d varies and passes through the critical value $d_0 = 1.1713341066595535$, system (2) undergoes a Hopf bifurcation at the equilibrium point

$$A_2 = (\frac{1}{20}(\sqrt{2}\sqrt{d^2 + 20} + \sqrt{2}d),$$
$$\frac{1}{10}(-\sqrt{d^2 + 20} - d), -\frac{1}{5\sqrt{2}}). \quad (7)$$

Firstly, we review the projection method presented in Chapters 3 and 5 of [42], but following the approach of [43]–[45], to compute the first Lyapunov coefficient L_1, connected with the stability of a Hopf bifurcation.

Consider the following differential equation

$$\dot{X} = f(X, \mu), \quad (8)$$

where $X \in \mathcal{R}^3$ and μ are respectively vectors representing phase variables and control parameters. We assume that f is

in a class of C^∞ functions in $\mathcal{R}^3 \times \mathcal{R}^2$. Suppose that (8) has an equilibrium $X = X_0$ at $\mu = \mu_0$. Denoting the perturbed variable $X - X_0$ by X, we write

$$F(X) = f(X, \mu_0), \quad (9)$$

as

$$F(X) = AX + \frac{1}{2}B(X, X) + \frac{1}{6}C(X, X, X) + o(\|X\|^4), \quad (10)$$

where

$$A = f_x(0, \mu_0),$$
$$B(X, Y) = \sum_{j,k=1}^{3} \frac{\partial^2 F_i(\xi)}{\partial^2 \xi_j \partial \xi_k}|_{\xi=0} X_j Y_k,$$
$$C(X, Y, Z) = \sum_{j,k,l=1}^{3} \frac{\partial^3 F_i(\xi)}{\partial \xi_j \partial \xi_k \partial \xi_l}|_{\xi=0} X_j Y_k Z_l. \quad (11)$$

Assume that A has a pair of complex eigenvalues on the imaginary axis: $\lambda_{2,3} = \pm \omega_0(\omega_0 > 0)$, and that these eigenvalues are the only eigenvalues with $\Re(\lambda) = 0$. Let T^c be the generalized eigenvalues of A corresponding to $\lambda_{2,3}$. Let $p, q \in C^3$ be vectors such that

$$Aq = i\omega_0 q, \quad A^T p = -i\omega_0 p, \quad \langle p, q \rangle - 1, \quad (12)$$

where A^T is the transpose of the matrix A. Any vector $y \in T^c$ can be expressed as $y = \omega q + \bar{\omega}\bar{q}$, where $\omega = \langle p, y \rangle \in C$. The two-dimensional center manifold related to the eigenvalues $\lambda_{2,3}$ can be parameterized by ω and $\bar{\omega}$, by way of an immersion of the form $X = H(\omega, \bar{\omega})$, where $H : \mathbb{C}^2 \to \mathcal{R}^2$ has a Taylor expansion of the following form

$$H(\omega, \varpi) = \omega q + \varpi \bar{q} + \sum_{2 \leq j+k \leq 3} \frac{1}{j!k!} h_{jk}\omega^j \varpi^k + o(|\omega|^4), \quad (13)$$
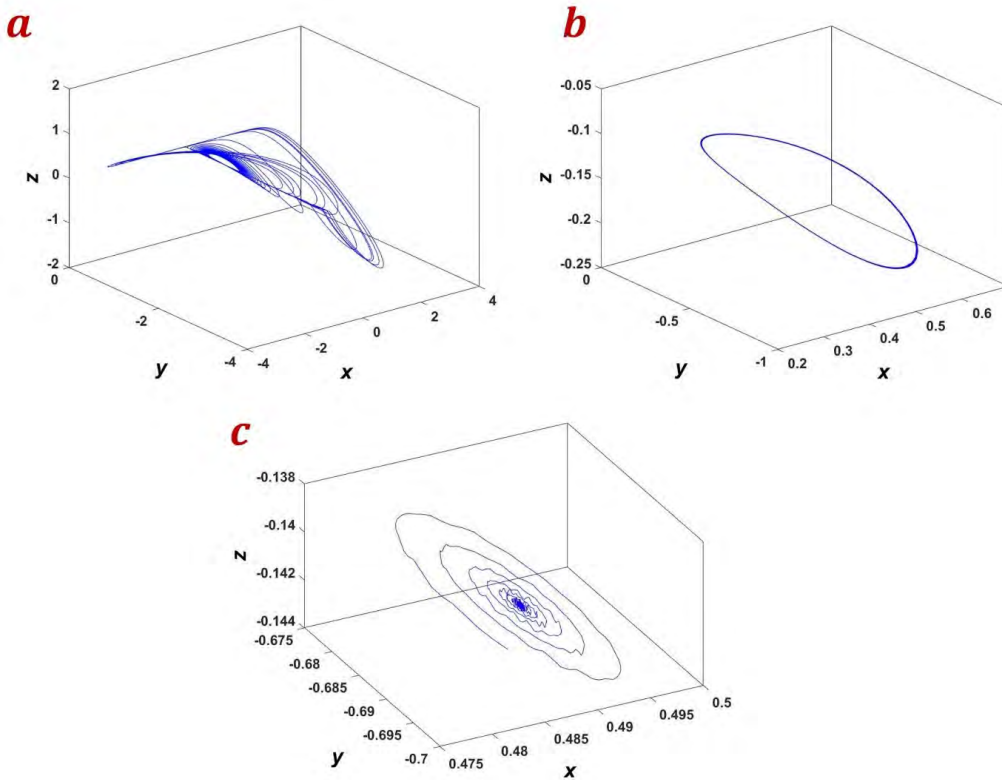
with $h_{jk} \in C^3$ and $h_{jk} = \bar{h}_{kj}$. Substituting this expression into (8) we get the following differential equation

$$H_\omega \omega' + H_\omega \varpi' = F(H(\omega, \varpi)), \quad (14)$$

where F is given by (9). The complex vectors H_{ij} are obtained from the coefficients of (14). Using the coefficients of F, system (14) can be written in the following form on the chart w for a central manifold,

$$\dot{\omega} = i\omega_0 \omega + \frac{1}{2}G_{21}\omega|\omega|^2 + o(|\omega|^4),$$

FIGURE 2. Occurrence of the Hopfs bifurcation phenomenon in the NCS system for $a = 0.2$, $b = 0.1$, $c = 0$ initial conditions $[0.3, -0.4, -0.1]$ showing stable oscillations for $d = 2$ (Fig.2c), periodic orbit from Hopf bifurcation for $d = 1.175 = d_0$ as in Fig.2b and chaotic oscillations for $d = 1.2$ as in Fig.2a.

with $G_{21} \in \mathbb{C}$. The first Lyapunov coefficient is given by $l_1 = \frac{1}{2}\Re(G_{21})$, where

$$G_{21} = \langle p, C(q, q, \bar{q}), B(\bar{q}, h_{20}) + 2B(q, h_{11}) \rangle.$$

If the Jacobian matrix A of a equilibrium point has only a pair of pure imaginary eigenvalues $\pm i\omega_0$, for $\omega_0 > 0$, with the other eigenvalues having nonzero real parts, then the equilibrium point is called a Hopf bifurcation point (X_0, μ_0). A two-dimensional center manifold is well defined at a Hopf point. Also, under the flow generated by (8), it is invariant and any higher-order derivatives can be continued to nearby parameter values.

Here we employ the three dimensional Hopf bifurcation method and use symbolic algebra calculations to analyze the parametric variations with respect to dynamic bifurcations. We consider the bifurcation of the system at

$$A_2(\frac{1}{20}(\sqrt{2}\sqrt{d^2 + 20} + \sqrt{2}d),$$

$$\frac{1}{10}(-\sqrt{d^2 + 20} - d), -\frac{1}{5\sqrt{2}}). \quad (15)$$

Theorem 2: The first Lyapunov coefficient, associated with A_2 is $l_1 = 0.759987$. The Hopf at A_2 is therefore subcritical giving an unstable (weak repelling focus). For each $d > d_0 = 1.1713341066595535$, in the neighbourhood of d_0, there is an unstable limit cycle around the asymptotically stable equilibrium point A_2.

proof: The transversality condition (6) is clearly satisfied. Accordingly, a Hopf bifurcation occurs at the equilibrium point. The sign of the first Lyapunov coefficient, l_1, determines the stability of the equilibrium point. Using the notation of the previous section, the multilinear symmetric functions are:

$$B(x, y) = (-x_2y_3 - x_3y_2, x_1y_3 + x_3y_1, x_1y_2$$

$$+ x_2y_1 + d(x_3y_2 + x_2y_3)), \quad C(x, y, z) = (0, 0, 0). \quad (16)$$

Furthermore, we also obtain

$$p = (-0.0709355 + 0.82177i, -0.677446$$
$$+ 0.00734658i, -0.22862 + 0.24996i),$$
$$q = (0.0521326 + 0.671851i, -0.692554,$$
$$- 0.151036 - 0.20846i),$$
$$h_{11} = (-0.913495 - 1.00648i, 0.552236$$
$$+ 1.42337i, 0.541569),$$
$$h_{20} = (-0.909752 + 0.572633i, -0.571446$$
$$- 1.09957i, 0.299607 - 0.249041i),$$
$$G_{21} = 1.51997 + 0.429021i, \quad (17)$$

so that $l_1 = 0.759987$. Theorem 2 is therefore proved.

To show the occurrence of Hopf bifurcations in the NCS, we have plotted the 3D phase portraits for $a = 0.2$,
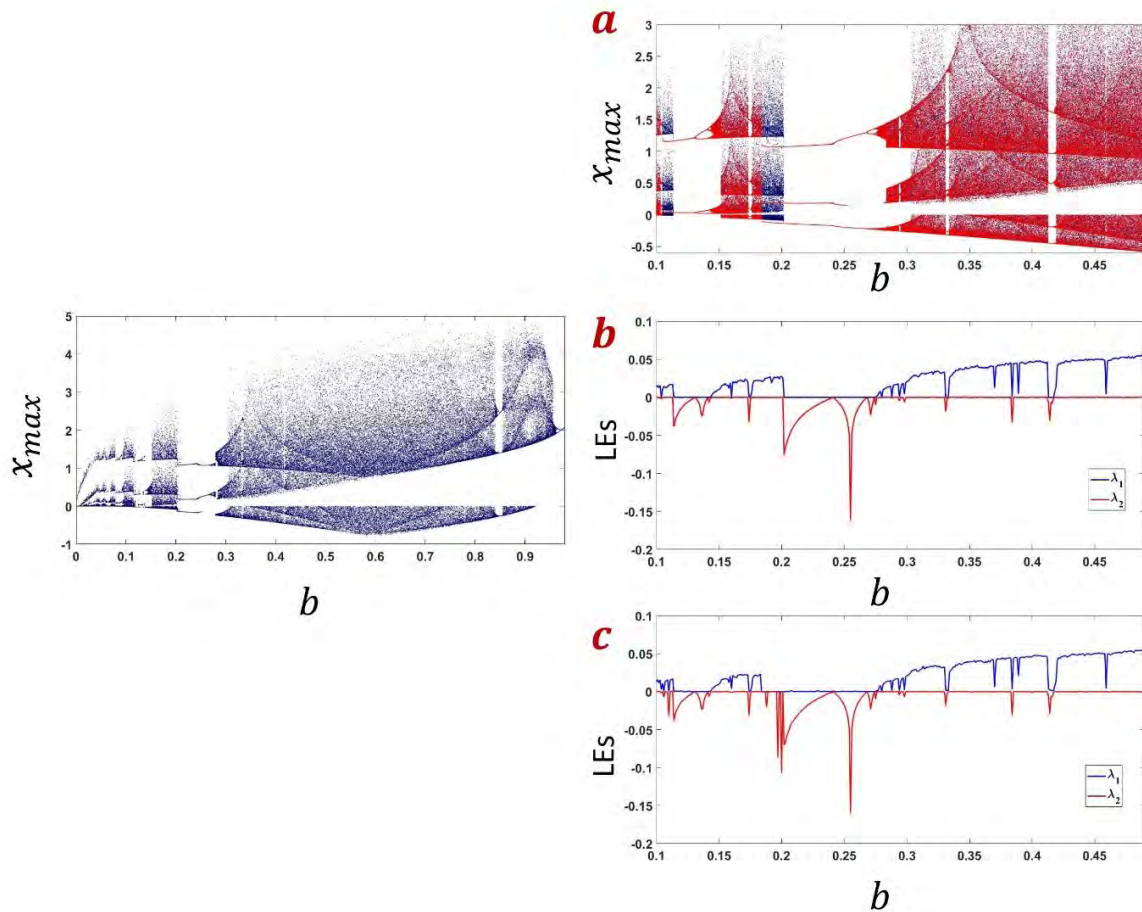
FIGURE 3. (left): Bifurcation of the NCS (case-1) with parameter *b*; Fig.3 (right) a: Bifurcation of the NCS (case-1) with parameter *b* with forward (blue) and backward (red) continuation in (b). The LEs of the system for forward continuation (c): The LEs of the system for backward continuation.

$b = 0.1, c = 0$ initial conditions $[0.3, -0.4, -0.1]$ and different values of d as shown in Fig.2. We see the bifurcating limit cycle from the Hopf bifurcation shown in Fig.2b, converting to a chaotic attractor for $d > d_0$ in Fig.2a.

V. BIFURCATION TRANSITION DIAGRAMS AND MULTISTABILITY

To study the dynamical behavior of the NCS with change in parameter, we obtain and investigate the bifurcation plots. Three different cases (A,B,C) are studied depending on the choice of parameters. The initial conditions are taken as $[0.1, 0.1, 0]$ and the local maxima of the state variable is plotted for different values of the control parameter to obtain the bifurcation diagrams. The multistability plots are derived using the well-known continuation method where the parameter is increased (forward) or decreased (backward), reinitializing the end conditions as initial conditions for the next parameter change. The local maxima of the state variable are plotted for each parameter increment/decrement.To calculate the finite time Lyapunov exponents (LEs), we used the Wolf's algorithm [41]. Initial conditions are saved during the

plotting of the multistability plots using forward and backward continuation.

Case A: Case A is Case-1 in which we chose the parameter values $a = 0.2, c = 0$ and $d = 0$, while parameter b is varied from 0 to 1. Fig.3 (left) shows the bifurcation transition diagram. For $0.10 < b < 0.11, 0.15 < b < 0.20, 0.28 < b < 0.42, 0.425 < b < 0.84$ and $0.86 < b < 0.98$ the NCS system shows chaotic oscillations. The system takes a period doubling route to chaos in the regions $0.25 < b < 0.28$ and $0.13 < b < 0.15$. Fig.3 (right) shows multistability plots, together with their respective LEs. The blue plots show the forward continuation and red plots show the backward continuation as in Fig.3a. We see the coexistence of a period-3 limit cycle with a chaotic attractor for the region $0.18 < b < 0.20$. The presence of coexisting attractors is confirmed by the corresponding LEs plots, shown in Fig.3b (forward) and Fig.3c (backward).

Case B: The parameter values for this case (not shown in Table 1) are $b = 0.1, c = 0.1$ and $d = 0$ with parameter a now varying from 0.1 to 0.14. Fig.4 (left) shows the bifurcation transition plot of the NCS as a function of a. For the regions, $0.101 < a < 0.105$ and $0.109 < a < 0.13$ the NCS
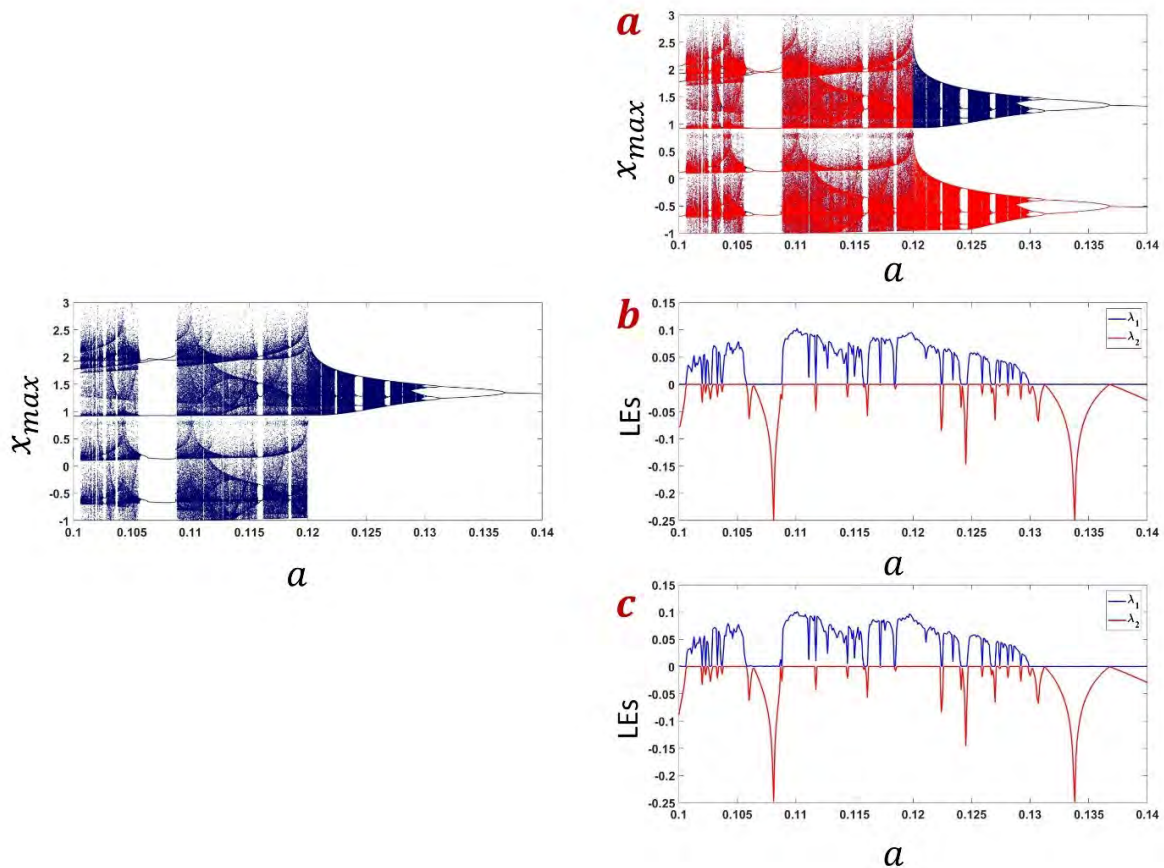
FIGURE 4. (left): Bifurcation of the NCS with parameter *a*; Fig.4 (right) (a): Bifurcation of the NCS with parameter *a* with forward (blue) and backward (red) continuation; (b): The LEs of the system for forward continuation; (c): The LEs of the system for backward continuation.

shows chaotic oscillations. The system now takes the route of period halving bifurcations from chaos, as seen for the range $0.130 < a < 0.137$. Fig.4 (right) shows multistability plots derived with forward (blue) and backward (red) continuation with the corresponding LEs shown in Fig.4b and 3c. In Fig. 4a we see two coexisting attractors for $0.12 < a < 0.13$, which is again confirmed by the corresponding LEs plots, shown in Fig.4b and 3c for forward and backward continuation respectively.

Case C: Case C is Case 5 of Table 1. The parameter values chosen are $a = 0.1$, $b = 0.1$ and $c = 0.001$, while d is varied from 0 to 0.7. Fig.5 (left) shows the bifurcation transition plot of the NCS with parameter, and, as can be seen from the figure the regions $0 < d < 0.105$ and $0.5 < d < 0.7$ are found to be chaotic. The system shows a period-doubling route to chaos, as seen in the region $0.38 < b < 0.47$. Fig.5 (right) shows the bifurcation diagrams with forward (blue) and backward (red) iterations with the corresponding LEs. We see multiple regions of coexisting chaotic attractors. As shown in Fig.5a, for $0.19 < b < 0.28$, chaotic attractors coexist with periodic limit cycles. This is confirmed by the corresponding LEs plots, shown in Fig.5b for forward continuation and Fig.5c for backward continuation.

The coexisting attractors [46] of the NCS system for the cases A and B are shown in Fig.6. We could see the symmetric attractors and coexisting limit cycles of the NCS system as correlated with the respective bifurcation plots shown in Fig.3 and Fig.4 respectively.

To show the coexistence of different attractors, we have plotted the basins for case-2 and case-4 as shown in Fig.7a and 7b respectively. The NCS system shows two symmetric chaotic attractors for each case as we have taken the mean value of the state y to separate the attractors. The negative chaotic attractor is plotted by cyan colour and the positive by magenta. In Fig.7a we see that case-2 goes to a fixed point only for the initial conditions [0, 0, 0] shown in red. In case-4, the system shows a line where evolution is to equilibria, shown in red in Fig.7b. Also there is a line, shown in yellow, where the system goes to infinity.

VI. BIFURCATION DIAGRAMS AND CASES IN TABLE 1
Our objective now is to learn how the various cases of system (2), as listed in Table 1, correspond to parts of the bifurcation transition diagrams as the parameter *c* varies. We note that when $d = 0$, system (2) is invariant under the symmetry $(x, y, z) \rightarrow (-x, -y, z)$. This means that phase diagrams of
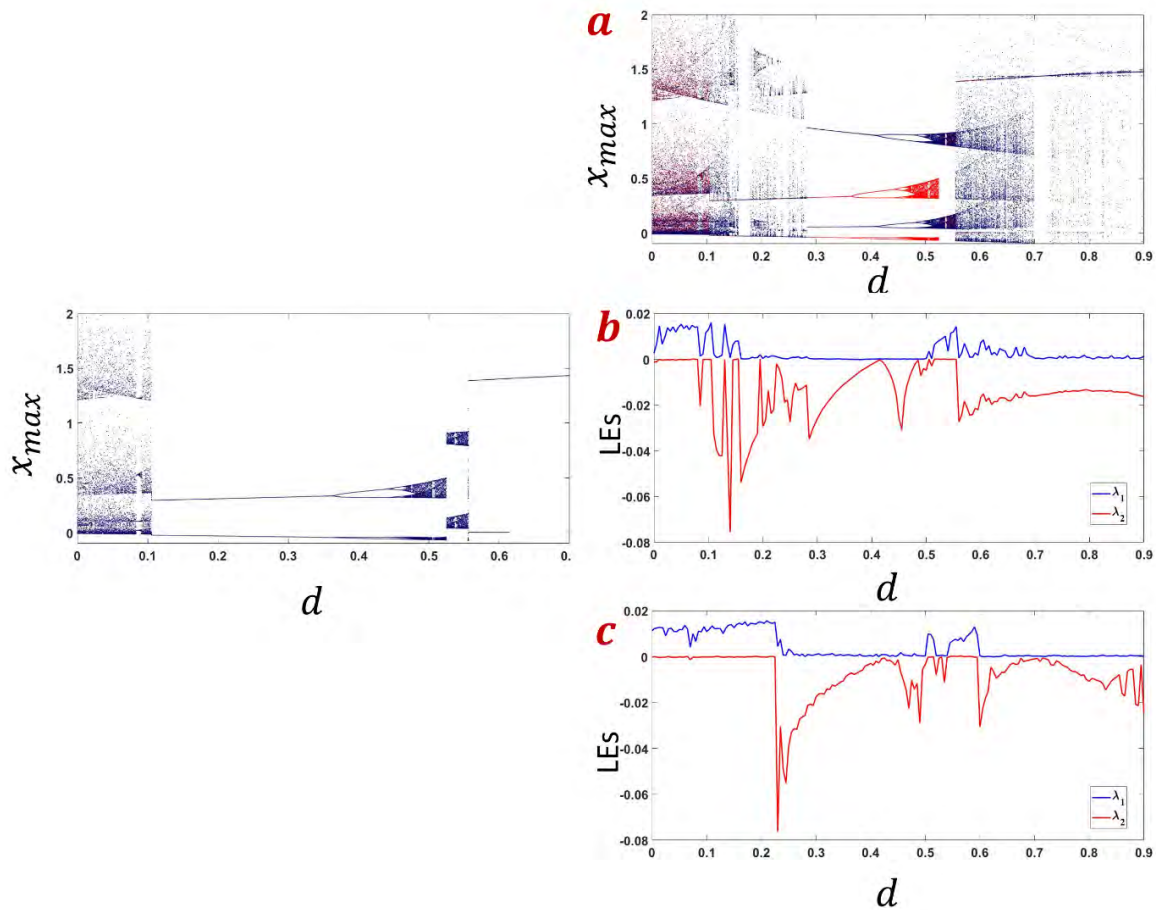
FIGURE 5. (left): Bifurcation of the NCS with parameter *d*; Fig.5 (right) a: Bifurcation of the NCS with parameter *d* with forward (blue) and backward (red) continuation; b: The LEs of the system for forward continuation; c: The LEs of the system for backward continuation.

(x, y) should exhibit reflexional symmetry. This applies to Cases 1, 2 and 3. The remaining cases break this symmetry.

A. *A* = 0.12, *B* = 0.1, *D* = 0

In Table 1, $b = 0.1$ in nearly all the cases, except for Case 3, while $a = 0.12$ in three of the cases. We therefore chose $(a, b, d) = (0.12, 0.1, 0)$ and varied c to produce a comparison of a bifurcation transition diagram with a plot of the x equilibrium state (see Figure 8(a)). There is a small interval $0 \leq c < 0.11$ for which the equilibrium states are real. For $c \geq 0.11$, we find only purely imaginary equilibria (see Figure 8(b)). The various bands of chaotic attractors, shown in Figure 8(a), coincide with the absence of real equilibrium states for *NCS* and are examples of hidden attractors.

When $c = 0$, we find phase portraits similar to those shown for Case 1 in Fig. 1. As c is increased, we find examples of phase portraits, shown in Case 2. When $c = 1.2$, we find the phase portraits shown in Figure. 9, which resembles a very asymmetric version of Case 3. This falls within the chaotic band of the upper panel of Figure. 8 in which there are both positive and negative values of x_{max} in the transition diagram. When $c = 2$, we have the phase portraits shown

in Figure. 10. Here there are two bands with only negative values of x_{max}. This is an example which differs from any of the phase portraits shown for Cases 1-6 in Table 1.

The bifurcation transition diagram for $(a = 0.12, b = 0.1, d = 0)$ as c varies, therefore has examples of four different chaotic attractors, three of which are located where the only equilibrium states are purely imaginary [47].

B. *B* = 0.1, *C* = 0.001, *D* = 0.1

We now fix $(b, c, d) = (0.1, 0.001, 0.1)$ and increase a. The bifurcation transition diagram is now shown in Figure 11 for $0 \leq a \leq 1$. Real equilibrium states exist throughout this interval. From Table 1, we see that the Case 5 chaotic attractor is located in the narrow band of chaotic solutions near $a = 0.1$. The Case 6 attractor is located in the middle of the much larger chaotic regime.

VII. NONLINEAR FEEDBACK CONTROL

We now illustrate how nonlinear feedback control can drive the dynamics of system (2) to equilibrium, using the nontrivial equilibria of Case 1 and Case 5 as examples.
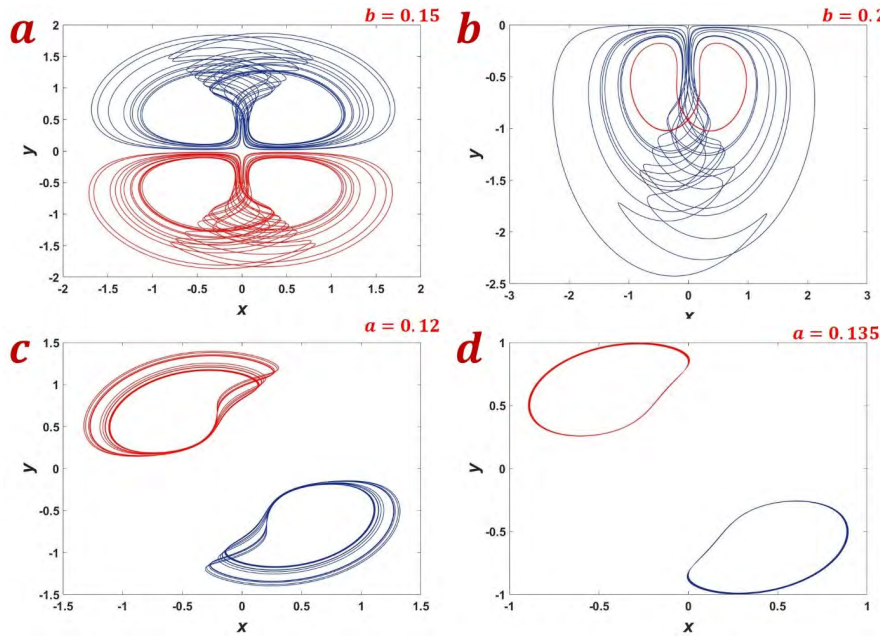
FIGURE 6. The coexisting attractors plotted for a) Case-A with blue plot showing phase portrait for initial conditions [0.10.10] and red plot for initial conditions [−0.1 − 0.10]; b) Case-A with blue plot showing phase portrait initial conditions [0.1 − 0.10] and red plot for [−0.1 − 0.10]; c) Case-B with blue plot showing the phase portrait for initial conditions [0.10.10] and red plot for initial conditions [−0.1 − 0.10]; d) Case-B with blue plot showing the phase portrait for initial conditions [0.10.10] and red plot for initial conditions [−0.1 − 0.10].
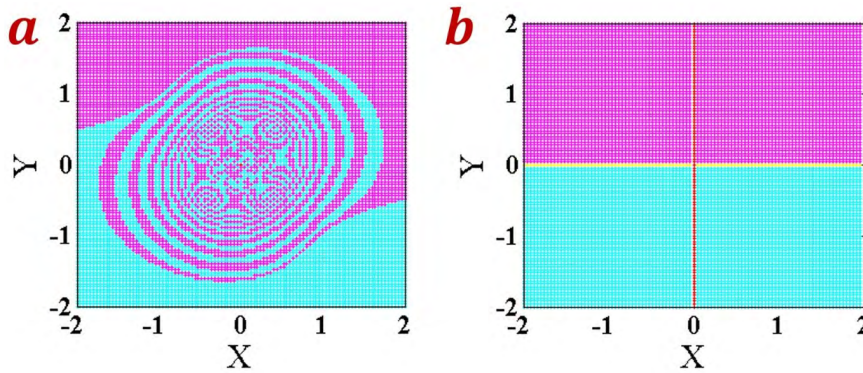
FIGURE 7. Basin of attraction of the NCS for a: Case-2; b: Case-4.

For nonlinear control, the first step is to include control signals u_1, u_2 and u_3 to the RHS of equations (2) to get:

$$dx/dt = ax - yz + u_1, \tag{18a}$$

$$dy/dt = -by + xz + u_2, \tag{18b}$$

$$dz/dt = c - z + xy + dzy + u_3. \tag{18c}$$

Writing the equilibrium state as $x_e = (x_e, y_e, z_e)$, we introduce error states as perturbations about x_e: $e_1 = x - x_e$, $e_2 = y - y_e$, $e_3 = z - z_e$. We substitute for x, y and z into eqns (18) to obtain a set of equations for e_1, e_2 and e_3:

$$de_1/dt = ae_1 - (e_2e_3 + y_ee_3 + z_ee_2) + u_1, \tag{19a}$$

$$de_2/dt = -be_2 + (e_1e_3 + z_ee_1 + x_ee_3) + u_2, \tag{19b}$$

$$de_3/dt = -e_3 + (e_1e_2 + y_ee_1 + x_ee_2)$$
$$+ d(e_2e_3 + y_ee_3 + z_ee_2) + u_3, \tag{19c}$$

where we have used $ax_e - y_ez_e = 0$, $-by_e + x_ez_e = 0$ and $c - z_e + x_ey_e + dy_ez_e = 0$.

The next step is to introduce the Lyapunov function

$$V(e_1, e_2, e_3) = \frac{1}{2}(e_1{}^2 + e_2{}^2 + e_3{}^2) \tag{20}$$

We note that V is positive definite, and our objective is to choose controls u_1, u_2 and u_3 to make dV/dt negative definite. This guarantees that the error system (19) decays asymptotically to zero, and so the system (18) converges to the chosen equilibrium state.
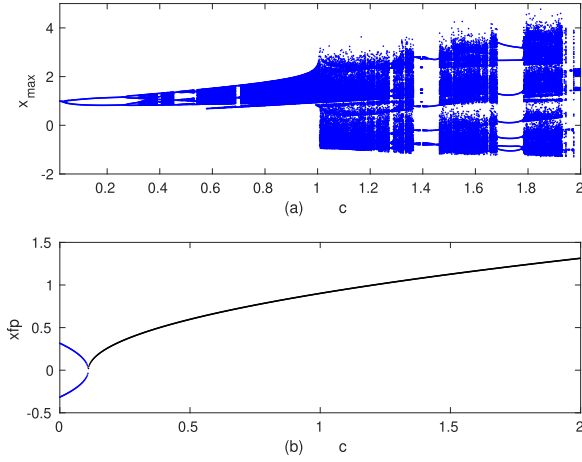
FIGURE 8. The upper figure shows the bifurcation transition diagram as parameter c varies for $(a, b, d) = (0.12, 0.1, 0)$, in terms of the maximum value of x over each cycle. The lower figure shows the real equilibrium point x (blue), and the imaginary part of x (black).
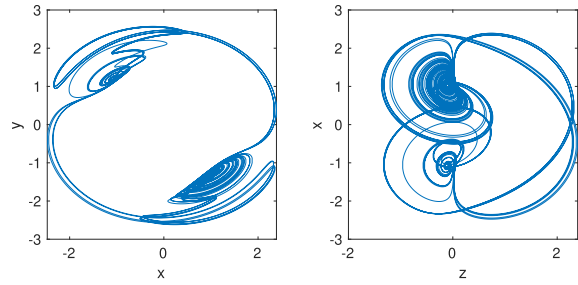
FIGURE 9. Phase portraits of (x, y) and (z, x) for $(a, b, c, d) = (0.12, 0.1, 1.2, 0)$. Note the similarity with Case 3.
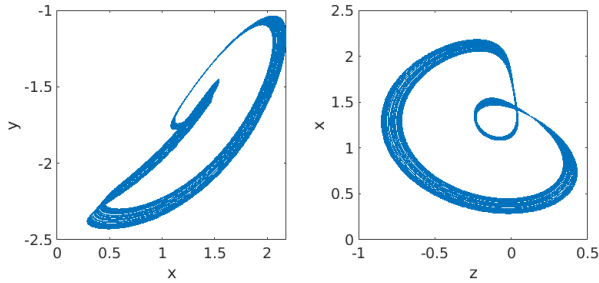
FIGURE 10. Phase portraits of (x, y) and (z, x) for $(a, b, c, d) = (0.12, 0.1, 2, 0)$.

Differentiating V wrt t, and substituting for $\dot{e}_1$, $\dot{e}_2$ and $\dot{e}_3$ gives, after some simplification:

$$\dot{V} = -(e_1{}^2 + be_2{}^2 + e_3{}^2) + (e_1{}^2(1 + a) + e_1 u_1)$$
$$+ e_2(2e_3 x_e + u_2) + e_3(de_2 e_3 + de_3 y_e + de_2 z_e + e_1 e_2). \quad (21)$$
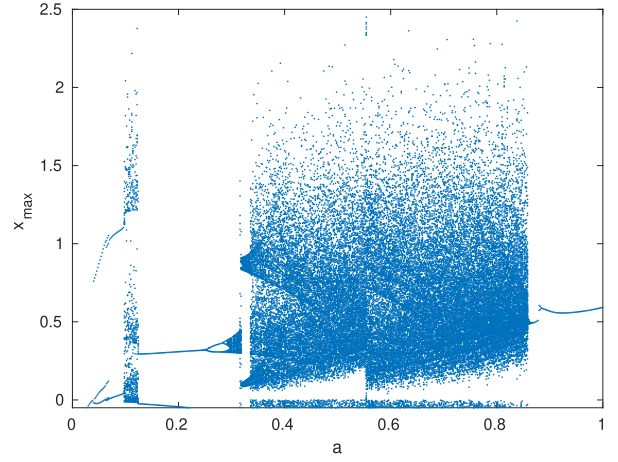
Choosing

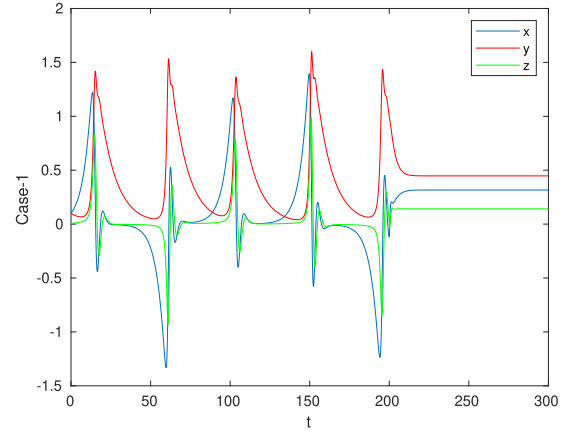$$u_1 = -(1 + a)e_1, \quad (22a)$$
$$u_2 = -2x_e e_3, \quad (22b)$$
$$u_3 = -d(e_2 e_3 + y_e e_3 + z_e e_2) - e_1 e_2, \quad (22c)$$

reduces (22) to

$$\dot{V} = -(e_1{}^2 + be_2{}^2 + e_3{}^2). \quad (23)$$

FIGURE 11. Bifurcation transition diagram as a increases for $(b, c, d) = (0.1, 0.001, 0.1)$.

FIGURE 12. The time series of x, y and z for parameter choices of Case-1. System (2) is integrated for the first 200 sec, before applying the control and switching to system (18) for the final 100 sec.

Since $b > 0$, $\dot{V}$ is negative definite, and system (18) evolves to the chosen equilibrium state.

We illustrate nonlinear feedback control using two of the cases listed in Table 1: Cases 1 and 5.

When $c = d = 0$ (Case 1), the nontrivial equilibrium state is given by $(x_e, y_e, z_e) = (\pm\sqrt{(b)}, \pm\sqrt{(a)}, \sqrt{(ab)})$, so that for $a = 0.2$ and $b = 0.1$, we obtain $(x_e, y_e, z_e) = (\pm 0.3162, \pm 0.4472, 0.1414)$. We set $(x_e, y_e, z_e) = (0.3162, 0.4472, 0.1414)$, and take initial conditions of $(0.1, 0.1, 0)$, to integrate the uncontrolled system (2) numerically for 200 sec with a time step of 0.01 sec, before switching to integrate equations (18) numerically for a further 100 sec.

Figure 12 shows the time series of x (blue), y (red) z (green) of system (2), evolving to the equilibrium state $(x_e, y_e, z_e) = (0.3162, 0.4472, 0.1414)$.

Figure 13 shows the corresponding nonlinear feedback control for the four nontrivial equilibria of Case 5. Panel (a) corresponds to the equilibrium $(0.3228, -0.3228, -0.1)$, panel (b) to $(-0.3128, 0.3128, -0.1)$, panel (c) to $(-0.3197, -0.3197, 0.1)$, and panel (d(to $(0.3097,$

FIGURE 13. The time series of *x*, *y* and *z* for parameter choices of Case-1. System (2) is integrated for the first 200 sec, before applying the control and switching to system (18) for the final 100 sec.
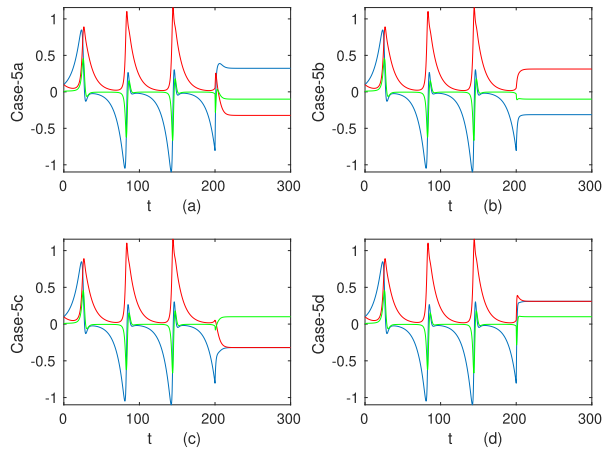
0.3097, 0.1). In all cases, the system evolves rapidly to the given equilibrium solution, once the nonlinear feedback control is applied.

VIII. CONCLUSIONS

In this paper, a simple chaotic system with topologically different attractors is examined with phase portraits. The system has self-excited attractor with five equilibrium points which give the topological difference to this system as compared with other well-known systems like Lorenz and Rossler attractors, which have three and two equilibria respectively. The dynamic properties of the system are presented in detail, by numerical simulation. A Hopf bifurcation, bifurcation transition diagrams, showing multistability of the proposed novel system are investigated. The system is modified by adding an additional nonlinear term in the third state equation, thereby generating six different self-excited chaotic attractors, as given in Table 1. The proposed system shows topologically different attractors for all the six cases. Also, an engineering application of system are performed on two of the Cases of Table 1 for illustration. We used nonlinear feedback control to drive the system to equilibrium, in both cases. More different and interesting issues corresponding to these topics will be addressed in future work.

REFERENCES

[1] E. N. Lorenz, "Deterministic nonperiodic flow," *J. Atmos. Sci.*, vol. 20, no. 2, pp. 130–141, 1963.

[2] E. Ott, *Chaos in Dynamical Systems*. Cambridge, U.K.: Cambridge Univ. Press, 2002.

[3] S. Wiggins, *Introduction to Applied Nonlinear Dynamical Systems and Chaos*, vol. 2. New York, NY, USA: Springer, 2003.

[4] H. Shao-Bo, S. Ke-Hui, and Z. Cong-Xu, "Complexity analyses of multiwing chaotic systems," *Chin. Phys. B*, vol. 22, no. 5, 2013, Art. no. 050506.

[5] L. Zhang, K. Sun, S. He, H. Wang, and Y. Xi, "Solution and dynamics of a fractional-order 5-D hyperchaotic system with four wings," *Eur. Phys. J. Plus*, vol. 132, p. 31, Jan. 2017.

[6] W. Ai, K. Sun, and Y. Fu, "Design of multiwing-multiscroll grid compound chaotic system and its circuit implementation," *Int. J. Mod. Phys. C*, vol. 29, no. 6, 2018, Art. no. 1850049.

[7] J. Chen, J. Sun, M. Chi, and X.-M. Cheng, "A novel scheme adaptive hybrid dislocated synchronization for two identical and different memristor chaotic oscillator systems with uncertain parameters," *Abstr. Appl. Anal.*, vol. 2014, Jan. 2014, Art. no. 675840.

[8] B. Bao, L. Xu, Z. Wu, M. Chen, and H. Wu, "Coexistence of multiple bifurcation modes in memristive diode-bridge-based canonical Chua's circuit," *Int. J. Electron.*, vol. 105, no. 7, pp. 1159–1169, 2018.

[9] H. Bao, N. Wang, H. Wu, Z. Song, and B. Bao, "Bi-stability in an improved memristor-based third-order Wien-bridge oscillator," *IETE Tech. Rev.*, vol. 36, no. 2, pp. 109–116, Jan. 2018.

[10] B. Bao, T. Jiang, G. Wang, P. Jin, H. Bao, and M. Chen, "Two-memristor-based Chua's hyperchaotic circuit with plane equilibrium and its extreme multistability," *Nonlinear Dyn.*, vol. 89, no. 2, pp. 1157–1171, 2017.

[11] S. He, K. Sun, and H. Wang, "Complexity analysis and DSP implementation of the fractional-order lorenz hyperchaotic system," *Entropy*, vol. 17, no. 12, pp. 8299–8311, Dec. 2015.

[12] J. Sun, Q. Yin, and Y. Shen, "Compound synchronization for four chaotic systems of integer order and fractional order," *Europhys. Lett.*, vol. 106, no. 4, p. 40005, 2014.

[13] S. He, C. Li, K. Sun, and S. Jafari, "Multivariate multiscale complexity analysis of self-reproducing chaotic systems," *Entropy*, vol. 20, no. 8, p. 556, 2018.

[14] Z. Wei, V.-T. Pham, A. J. M. Khalaf, J. Kengne, and S. Jafari, "A modified multistable chaotic oscillator," *Int. J. Bifurcation Chaos*, vol. 28, no. 7, 2018, Art. no. 1850085.

[15] Y.-X. Tang, A. J. M. Khalaf, K. Rajagopal, V.-T. Pham, S. Jafari, and Y. Tian, "A new nonlinear oscillator with infinite number of coexisting hidden and self-excited attractors," *Chin. Phys. B*, vol. 27, no. 4, 2018, Art. no. 040502.

[16] B. Bao, T. Jiang, Q. Xu, M. Chen, H. Wu, and Y. Hu, "Coexisting infinitely many attractors in active band-pass filter-based memristive circuit," *Nonlinear Dyn.*, vol. 86, no. 3, pp. 1711–1723, 2016.

[17] B. C. Bao, Q. Xu, H. Bao, and M. Chen, "Extreme multistability in a memristive circuit," *Electron. Lett.*, vol. 52, no. 12, pp. 1008–1010, 2016.

[18] M. Chen, M. Sun, B. Bao, H. Wu, Q. Xu, and J. Wang, "Controlling extreme multistability of memristor emulator-based dynamical circuit in flux–charge domain," *Nonlinear Dyn.*, vol. 91, no. 2, pp. 1395–1412, 2018.

[19] D. Dudkowski, S. Jafari, T. Kapitaniak, N. V. Kuznetsov, G. A. Leonov, and A. Prasad, "Hidden attractors in dynamical systems," *Phys. Rep.*, vol. 637, pp. 1–50, Jun. 2016.

[20] Y. Feng, Z. Wei, U. E. Kocamaz, A. Akgul, and I. Moroz, "Synchronization and electronic circuit application of hidden hyperchaos in a four-dimensional self-exciting homopolar disc dynamo without equilibria," *Complexity*, vol. 2017, May 2017, Art. no. 7101927.

[21] Z. Wei, K. Rajagopal, W. Zhang, S. T. Kingni, and A. Akgül, "Synchronisation, electronic circuit implementation, and fractional-order analysis of 5D ordinary differential equations with hidden hyperchaotic attractors," *Pramana*, vol. 90, no. 4, p. 50, 2018.

[22] S. Ren, S. Panahi, K. Rajagopal, A. Akgul, V.-T. Pham, and S. Jafari, "A new chaotic flow with hidden attractor: The first hyperjerk system with no equilibrium," *Zeitschrift Naturforschung A*, vol. 73, no. 3, pp. 239–249, 2018.

[23] G. Leonov, N. Kuznetsov, and V. Vagaitsev, "Localization of hidden Chua's attractors," *Phys. Lett. A*, vol. 375, no. 23, pp. 2230–2233, 2011.

[24] N. V. Stankevich, N. V. Kuznetsov, G. A. Leonov, and L. O. Chua, "Scenario of the birth of hidden attractors in the Chua circuit," *Int. J. Bifurcation Chaos*, vol. 27, no. 12, 2017, Art. no. 1730038.

[25] N. V. Kuznetsov, G. A. Leonov, T. N. Mokaev, A. Prasad, and M. D. Shrimali, "Finite-time Lyapunov dimension and hidden attractor of the Rabinovich system," *Nonlinear Dyn.*, vol. 92, no. 2, pp. 267–285, 2018.

[26] G. A. Leonov, N. V. Kuznetsov, and T. N. Mokaev, "Hidden attractor and homoclinic orbit in Lorenz-like system describing convective fluid motion in rotating cavity," *Commun. Nonlinear Sci. Numer. Simul.*, vol. 28, nos. 1–3, pp. 166–174, 2015.

[27] N. K. G. Leonov and V. Vagaitsev, "Hidden attractor in smooth Chua systems," *Phys. D, Nonlinear Phenomena*, vol. 241, no. 18, pp. 1482–1486, 2012.

[28] V.-T. Pham, S. Vaidyanathan, C. K. Volos, S. Jafari, N. V. Kuznetsov, and T. M. Hoang, "A novel memristive time–delay chaotic system without equilibrium points," *Eur. Phys. J. Special Topics*, vol. 225, no. 1, pp. 127–136, 2016.

[29] S. T. Kingni, S. Jafari, H. Simo, and P. Woafo, "Three-dimensional chaotic autonomous system with only one stable equilibrium: Analysis, circuit design, parameter estimation, control, synchronization and its fractional-order form," *Eur. Phys. J. Plus*, vol. 129, no. 5, p. 76, 2014.

[30] V.-T. Pham, S. Jafari, C. Volos, A. Giakoumis, S. Vaidyanathan, and T. Kapitaniak, "A chaotic system with equilibria located on the rounded square loop and its circuit implementation," *IEEE Trans. Circuits Syst. II, Exp. Briefs*, vol. 63, no. 9, pp. 878–882, Sep. 2016.

[31] H. Bao, N. Wang, B. Bao, M. Chen, P. Jin, and G. Wang, "Initial condition-dependent dynamics and transient period in memristor-based hypogenetic jerk system with four line equilibria," *Commun. Nonlinear Sci. Numer. Simul.*, vol. 57, pp. 264–275, Apr. 2018.

[32] O. E. Rössler, "An equation for continuous chaos," *Phys. Lett. A*, vol. 57, no. 5, pp. 397–398, 1976.

[33] J. C. Sprott, "Some simple chaotic flows," *Phys. Rev. E, Stat. Phys. Plasmas Fluids Relat. Interdiscip. Top.*, vol. 50, no. 2, p. R647, 1994.

[34] C. Gissinger, E. Dormy, and S. Fauve, "Morphology of field reversals in turbulent dynamos," *Europhys. Lett.*, vol. 90, no. 4, p. 49001, 2010.

[35] J. Sun, X. Zhao, J. Fang, and Y. Wang, "Autonomous memristor chaotic systems of infinite chaotic attractors and circuitry realization," *Nonlinear Dyn.*, vol. 94, no. 4, pp. 2879–2887, 2018.

[36] J. Sun, G. Han, Y. Wang, H. Zhang, and L. Wu, "Hybrid memristor chaotic system," *J. Nanoelectron. Optoelectron.*, vol. 13, no. 6, pp. 812–818, 2018.

[37] H. Wu, Y. Ye, B. Bao, M. Chen, and Q. Xu, "Memristor initial boosting behaviors in a two-memristor-based hyperchaotic system," *Chaos, Solitons Fractals*, vol. 121, pp. 178–185, Apr. 2019.

[38] M. Chen, Y. Feng, H. Bao, B. C. Bao, Y. J. Yu, H. G. Wu, and Q. Xu, "State variable mapping method for studying initial-dependent dynamics in memristive hyper-jerk system with line equilibrium," *Chaos, Solitons Fractals*, vol. 115, pp. 313–324, Oct. 2018.

[39] B. C. Bao, H. Bao, N. Wang, M. Chen, and Q. Xu, "Hidden extreme multistability in memristive hyperchaotic system," *Chaos, Solitons Fractals*, vol. 94, pp. 102–111, Jan. 2017.

[40] C. Gissinger, "A new deterministic model for chaotic reversals," *Eur. Phys. J. B*, vol. 85, no. 4, p. 137, 2012.

[41] A. Wolf, J. B. Swift, H. L. Swinney, and J. A. Vastano, "Determining Lyapunov exponents from a time series," *Phys. D, Nonlinear Phenomena*, vol. 16, no. 3, pp. 285–317, 1985.

[42] Y. A. Kuznetsov, *Elements of Applied Bifurcation Theory* (Applied Mathematical Sciences). New York, NY, USA: Springer, 2004.

[43] L. F. Mello and S. F. Coelho, "Degenerate Hopf bifurcations in the Lü system," *Phys. Lett. A*, vol. 373, nos. 12–13, pp. 1116–1120, 2009.

[44] J. Sotomayor, L. F. Mello, and D. D. C. Braga, "Bifurcation analysis of the Watt governor system," *Comput. Appl. Math.*, vol. 26, no. 1, pp. 19–44, 2007.

[45] J. Sotomayor, L. F. Mello, and D. D. C. Braga, "Lyapunov coefficients for degenerate Hopf bifurcations," 2007, *arXiv:0709.3949*. [Online]. Available: https://arxiv.org/abs/0709.3949

[46] W. Liu, K. Sun, and S. He, "SF-SIMM high-dimensional hyperchaotic map and its performance analysiss," *Nonlinear Dyn.*, vol. 89, no. 4, pp. 2521–2532, 2017.

[47] M. Yu, K. Sun, W. Liu, and S. He, "A hyperchaotic map with grid sinusoidal cavity," *Chaos, Solitons Fractals*, vol. 106, pp. 107–117, Jan. 2018.

KARTHIKEYAN RAJAGOPAL received the master's degree in embedded system technologies with emphasis on real-time targets programming and the Ph.D. degree in electronics and communication engineering with specializing in chaos-based secure communication engineering. He is currently a Senior Research Member and a Professor with the Center for Nonlinear Dynamics, Defence University, Ethiopia. He has more than 100 international journal papers indexed in SCI. His current research interests include fractional order nonlinear systems and control, time delay systems, FPGA, and the LabVIEW implementations of fractional order systems.

AKIF AKGUL received the B.Sc. degrees in electronics-computer education from Kocaeli University, in 2009, and in electrical- electronics engineering from Sakarya University, in 2013, and the M.S. and Ph.D. degrees in electronics computer education and electrical-electronics engineering from Sakarya University, in 2011 and 2015, respectively. He has joined the Institute of Electronics, Communications and Information Technology (ECIT), Queen's University Belfast, U.K., in 2015 as a Visiting Researcher. His current interests include analog electronics, chaos theory, chaotic systems, chaos-based engineering applications (cryptography, steganography, and pseudo and true random number generators), experimental chaotic synchronization, analysis and design of analog circuits, and microcomputer-based applications.

IRENE M. MOROZ current research interests include comparisons between deterministic and stochastic parameterization schemes for both low order differential equations and the integrated forecasting system of the european centre for medium range weather forecasting, the bifurcation analysis of nonlinear ordinary differential equations, arising in dynamo models and low order models of plankton, especially in geophysical fluid dynamics, also, investigation of models for the synchronization between the Quasi-Biennial oscillation and the semi-annual mode.

ZHOUCHAO WEI received the B.Sc. degree in applied mathematics and the Ph.D. degree in applied mathematics from the South China University of Technology, in 2006 and 2011, respectively. He joined the College of Mechanical Engineering, Beijing University of Technology, in 2014 as a Postdoctoral Fellow, and also with the Faculty of Mechanical Engineering, Technical University of Lodz, Poland, in 2015 as a Visiting Researcher. He has also been as a Visiting Scholar with the Mathematical Institute, University of Oxford, U.K., from 2016 to 2017. He is currently a Professor with the China University of Geosciences, Wuhan, China. He has been supported by several National Natural Science Funds. He has published more than 50 relevant academic papers in SCOPUS-indexed journals. His current research interests include the qualitative theory of differential equations, chaotic theory, and bifurcation theory.

SAJAD JAFARI was born in Kermanshah, Iran, in 1983. He received the B.Sc., M.S., and Ph.D. degrees in biomedical engineering from the Biomedical Engineering Department, Amirkabir University of Technology, Tehran, Iran, in 2005, 2008, and 2013, respectively. He is currently an Assistant Professor. His research interests include artificial intelligence, optimization, and pattern recognition, especially nonlinear and chaotic signals and systems.

IQTADAR HUSSAIN received the Ph.D. degree in mathematics from Quaid-i-Azam University, Pakistan, in 2014. He is currently an Assistant Professor with Qatar University. His h-index score is 23 and i-10 index score is 34. His research interests include the applications of mathematical concepts in secure communication and cybersecurity. He has published 67 papers in well-known journals in these areas.

• • •